Journal of Colloid and Interface Science 545 (2019) 311–316

Contents lists available at ScienceDirect

Journal of Colloid and Interface Science

journal homepage: www.elsevier.com/locate/jcis

Editor's Choice

Novel applications of perovskite oxide via catalytic peroxymonosulfate advanced oxidation in aqueous systems for trace L-cysteine detection

Lihong Liu [a], Jun Gao [b], Pengyun Liu [a], Xiaoguang Duan [c], Ning Han [a], Fuping Li [a], M. Veronica Sofianos [d], Shaobin Wang [a,c,*], Xiaoyao Tan [e], Shaomin Liu [a,*]

[a] WA School of Mines: Minerals, Energy and Chemical Engineering, Curtin University, Perth, WA 6845, Australia
[b] School of Chemistry and Environmental Engineering, Shandong University of Science and Technology, Qingdao 266510, PR China
[c] School of Chemical Engineering, The University of Adelaide, Adelaide, SA 5005, Australia
[d] Department of Physics and Astronomy, Fuels and Energy Technology Institute, Curtin University, GPO Box U1987, Perth, WA 6845, Australia
[e] School of Environmental and Chemical Engineering, Tianjin Polytechnic University, China

GRAPHICAL ABSTRACT

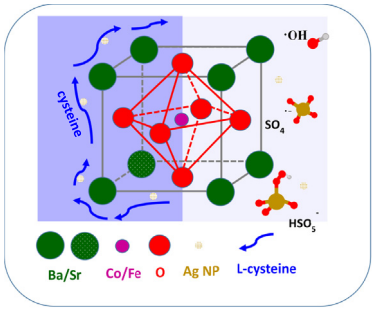

ARTICLE INFO

Article history:
Received 28 January 2019
Revised 11 March 2019
Accepted 13 March 2019
Available online 14 March 2019

Keywords:
Textile dyes, perovskite catalyst
Peroxymonosulfate
Catalytic oxidation
L-cysteine detection

ABSTRACT

Perovskite oxides offer new opportunities in wastewater treatment via catalytic oxidation. Herein, we report a new application of perovskite oxides for biological detection via catalytic decolourisation and colorimetric determination. The presence of trace biomolecules in an aqueous system would interfere the decolourisation process of dyes, where the decolourisation rate is quantitatively correlated to the biomolecular concentration. In this work, trace L-cysteine (Cys) detection was demonstrated on the basis of a Ag-$Ba_{0.5}Sr_{0.5}Co_{0.75}Fe_{0.2}O_{3-\delta}$ (Ag-BSCF)/peroxymonosulfate/textile dye system. Thiol-containing cysteine can bind to Ag, Co and Fe atoms, therefore shielding the catalytic performance of the perovskite in degradation of dye solutions. Such a cost-effective biosensor system presents an excellent linear response in Cys concentration ranging from nM to μM.

1. Introduction

Bioactive L-cysteine (Cys) plays several vital roles in human cellular functions. An abnormal level of Cys is usually associated with the risks of Alzheimer's diseases, skin lesions, liver damage, neurotoxicity, kidney failure, diabetes, thromboembolism, cerebrovascular/cardiovascular disorders and many others [1,2]. Consequently, an accurate quantification of Cys in biological and

* Corresponding authors at: WA School of Mines: Minerals, Energy and Chemical Engineering, Curtin University, Perth, WA 6845, Australia (S. Wang).
E-mail addresses: Shaobin.Wang@adelaide.edu.au (S. Wang), Shaomin.Liu@curtin.edu.au (S. Liu).

https://doi.org/10.1016/j.jcis.2019.03.045
0021-9797/

pharmaceutical samples has attracted considerable interest. Various analytical techniques have been developed for Cys detection including high-performance liquid chromatography, capillary electrophoresis, fluorescence spectrometry, UV–Vis absorption spectrophotometry and electrochemical analysis [3–10]. Among these methods, colorimetric sensing of Cys based on localised surface plasmon resonance (LSPR) of noble metal nanoparticles (NPs) or peroxidase-like activity of nanomaterials exhibits superior sensitivity and relative simplicity to the other instrumentation techniques [11].

Since the first report of intrinsic peroxidase-like activity of ferromagnetic nanoparticles, numerous nanomaterials have been exploited for H_2O_2 decomposition into ·OH radicals to oxidise the classical peroxidase substrate, 3,3,5,5-tetramethylbenzidine (TMB) [12]. The blue colour of oxidised TMB displays an excellent selectivity over non-thiolate amino acids, and glutathione can be detected up to 0.07 μM via colorimetric and fluorometric assays [13–15]. Another frequently used chromogenic substrate is 2,2′-Azinobis(3-ethylbenzothiazoline-6-sulfonic acid)-diammonium salt (ABTS). It develops green colour in 20 min upon reaction with horseradish peroxidase. However, the cost of these enzyme substrates is at least 25 times higher than industrial colouring stuff, like dyes.

Recently, Chen et al. and Xie et al. reported colorimetric determination of Cys by employing its inhibitory action on the peroxidase-like activity of Pt containing nanohybrids [16,17]. When the active sites of Pt nanoparticles (NPs) are blocked by the adsorption of Cys, less ·OH would be produced to oxidise the TMB, thus leading to lighter colour solution. Again, all such probes are expensive because they are predominantly composed of noble metals. Moreover, the enzyme assays depend decisively on defined conditions with respect to temperature, pH, nature and strength of ions, therefore, the detections need to be performed in special buffer solutions [18].

In the present study, we aimed to develop a fast, low cost and sensitive method for Cys determination in aqueous solutions by using $Ba_{0.5}Sr_{0.5}Co_{075}Fe_{0.2}O_{3-\delta}$ (BSCF) perovskite oxides. BSCF has been emerged as an advanced material for various applications including ceramic membranes for oxygen separation, cathode for solid oxide fuel cells, and a catalyst for oxygen reduction reaction [19–21]. Recently, our group discovered that BSCF and Ag-$La_{0.8}Ca_{0.2}Fe_{0.94}O_{3-\delta}$ could effectively activate peroxymonosulfate (PMS) to produce both ·OH and $SO_4^{\cdot-}$, therefore exhibiting a great efficiency in the degradation of a wide range of organic contaminants including different dyes [22,23]. Inspired by these works, Ag-$Ba_{0.5}Sr_{0.5}Co_{0.75}Fe_{0.2}O_{3-\delta}$ perovskite was explored for Cys detection. In addition to the good binding to Co and Fe [24,25], the high affinity of Cys for the Ag {1 1 1} facet is well known [26], thus the sensing strategy is based on the target-induced shielding against the peroxidase-like activity of the perovskite. To the best of our knowledge, no literature has been reported in the perovskite oxide for colorimetric detection of Cys. This is the first report in using these perovskite oxides for the applications in biological analysis.

2. Experimental

2.1. Perovskite oxide synthesis

All chemicals were of at least analytical grade purchased from Sigma-Aldrich (Australia) and used as received without further purification. The B-site deficient perovskite oxide, $Ba_{0.5}Sr_{0.5}Co_{0.75}Fe_{0.2}O_{3-\delta}$, was prepared via a classic sol–gel method followed by calcination. Firstly, metal nitrates such as $Ba(NO_3)_2$, $Sr(NO_3)_2$, $Co(NO_3)_2{\cdot}6H_2O$ and $Fe(NO_3)_3{\cdot}9H_2O$ with a molar ratio of 0.5:0.5:0.75:0.2 were dissolved in a mixture of deionised water, citric acid (CA) and EDTA to form a homogeneous solution at CA: EDTA:total metal ions = 1.5:1.0:1.0 (molar ratio). The pH value of the solution was adjusted to around 8 with ammonium solution or nitric acid to avoid precipitation. The solution was heated at 80 °C to evaporate water and produce a transparent gel. The gel was pre-treated at 250 °C for 5 h to get a powder precursor, subsequently calcined at 800 °C for 4 h in static air to remove the residual nitrates/carbonates and finally formed into perovskite oxide crystals. This sample was referred as BSCF800.

In a similar manner, silver incorporated Ag-$Ba_{0.5}Sr_{0.5}Co_{0.75}Fe_{0.2}O_{3-\delta}$ was synthesised by adding a suitable amount of $AgNO_3$ in a solution with the final molar ratio of 0.5 Ba:0.5 Sr:0.75 Co:0.2 Fe:0.05 Ag. The obtained powder precursor was also calcined at 800 °C (Ag-BSCF800) or 900 °C (Ag-BSCF900) prior to the wet ball-milling at 500 rpm in ethanol for 5 h in order to decrease the particle agglomeration during the calcination. Silver has a melting point of 962 °C. As soon as Ag melts, it will start to evaporate to a significant extent. To prevent the precious metal loss, we did not calcine the sample at a higher temperature.

2.2. Characterisation

The sample morphology was characterised by using a transmission electron microscope (TEM, JEOL EM-2100). High angle annular dark field scanning transmission electron microscopy (HAADF-STEM) imaging and elemental mapping were carried out using a FEI Titan G2 80-200 TEM/STEM with ChemiSTEM Technology operating at 200 kV. The elemental maps were obtained by energy dispersive X-ray spectroscopy using the Super-X detector on the Titan with a probe size of 1 nm and a probe current of 0.4 nA. X-ray diffraction analysis was performed on a Bruker D8 Advance X-ray Diffractometer with a Cu Kα radiation. The diffraction intensities were recorded at 2θ from 20° to 80°. X-ray photoelectron spectra (XPS) were recorded using a PHI 5000 VersaProbe spectrometer with an Al-Kα X-ray gun. All of the binding energies were calibrated using carbon (C 1s) at 284.6 eV as a reference. The electron paramagnetic resonance (EPR) signals of 5, 5-dimethyl-1-pyrroline (DMPO) adducts were detected at the ambient temperature with a Bruker (E500) spectrometer. The irradiation source was a Quanta-Ray Nd:YAG pulsed laser system (k = 532 nm, 10 Hz). The settings for the EPR spectrometer were as follows: centre field = 3515 G; sweep width = 100 G; microwave power = 18.51 mW, attenuation = 10 dB, receiver gain = 30 dB, scan time = 30 s, and scan number = 3.

2.3. Colorimetric detection of L-cysteine

Typically, 50 μL catalyst (Ag-BSCF900, 0.5 g/L), 50 μL of various concentrations of L-cysteine, 500 μL of methylene blue (MB, 20 ppm) or 600 μL of Rhodamine 6G (Rho6G, 20 ppm) and 10 μL of PMS (50 mM) were mixed and incubated at room temperature for 3 min, followed by centrifugation at 8000 rpm for 1 min, and then 200 μL solution was transferred to a 96-well plate for MB and Rho6G absorbance measurement at 664 and 529 nm, respectively (EnSpire benchtop multimode plate reader, PerkinElmer).

3. Results and discussion

XRD patterns of the prepared powders are presented in Fig. 1A. The Bragg diffraction peaks of $Ba_{0.5}Sr_{0.5}Co_{0.75}Fe_{0.2}O_{3-\delta}$ (a, sintered at 800 °C for 4 h) are corresponding to the (1 0 0), (1 1 0), (1 1 1), (2 0 0), (2 1 0), (2 1 1), (2 2 0) and (3 1 0) lattice planes of the pure BSCF perovskite phase [27]. For silver containing samples, additional peaks at 38.2° and 44.4° are observed to be indexed to the (1 1 1) and (2 0 0) planes of metallic Ag [28]. The morphologies

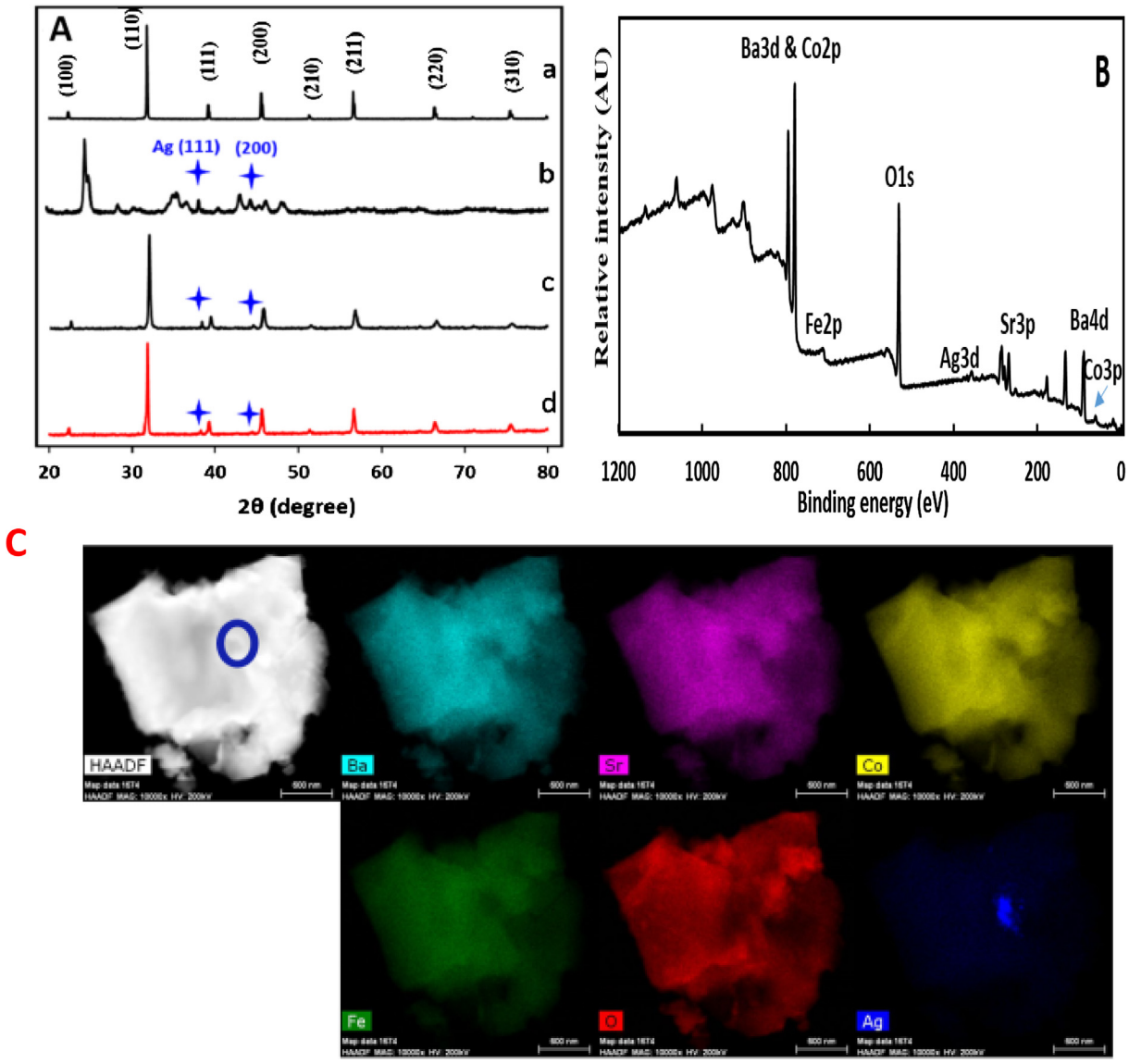

Fig. 1. X-ray diffraction patterns (A) of the prepared samples [a, BSCF800; b, Ag-BSCF powder precursor after heat treatment at 250 °C for 5 h; c, Ag-BSCF800; d, Ag-BSCF900], XPS survey of Ag-BSCF900 (B); typical HAADF-EDX elemental mapping of Ag-BSCF900 (C). Scale bars: 600 nm.

of Ag-BSCF perovskite were revealed by a FESEM (Fig. S1). The particle size was less than 2 μm, with evident needle-like nanocrystallite agglomeration.

XPS survey-scan spectrum reveals that the sample consists of only Ba, Ca, Sr, Co, Fe, O, and Ag elements (Fig. 1B). The main peaks with a binding energy (BE) value at 780.1 eV are assigned to both $Co_{2p3/2}$ and $Ba_{3d5/2}$. The Fe2p core level spectrum gives two BE peaks at 723.3 and 710.0 eV, which can be assigned to $Fe2p_{1/2}$ and $Fe2p_{3/2}$ of Fe^{3+}, respectively [29]. High-angle annular dark-field (HAADF) scanning transmission electron microscopy (STEM) combined with energy-dispersive X-ray (EDX) spectroscopy of the Ag-BSCF900 (Fig. 1c) shows that the constituent elements are uniformly distributed throughout the particles. Ag NPs are anchored on the surface of the host perovskite (Fig. 1c). Cys molecules are assumed to be chemisorbed on Ag NPs, therefore inactivate PMS reduction and decrease the rate of dye decolourisation, which will be discussed further subsequently.

All prepared powders were firstly evaluated for the sensitivity of Cys detection through decolourisation of methylene blue (MB) in the presence of PMS. Without Cys, under conditions as listed in Fig. 2A, we found that all the samples calcined at or above 800 °C can completely decompose MB within 15 min. BSCF powder precursor had no obvious effect on PMS reduction and MB degradation. The addition of Cys apparently slows down the MB degradation rate. The absorption difference ($\Delta A = A_0 - A_1$, where A_0 and A_1 are the absorbance at 664 nm of the reaction solutions in the absence and presence of Cys, respectively) is used to screen the most effective perovskite materials. Clearly, Ag-BSCF900 provided the maximum absorption difference (ΔA) of 0.45. Moreover, the method presents a linear response of Cys concentration in the ranges of 0.16–1.6 μM (Fig. 2B), 1.6–86 μM (Fig. 2C) and 86–322 μM (Fig. 2D). The dependence between ΔA_{664} and Cys concentration (x, in μM) can be expressed by the linear regress equations with all R^2 higher than 0.99 (Fig. 2).

To simplify the operation, we further investigated the direct correlation between absolute A_{664} (the solution absorbance at 664 nm) versus [Cys], instead of ΔA_{664} versus [Cys]. The results displayed in Fig. 3 dynamically indicate the perovskite catalyst content has a critical impact on the linear response of lg (L-cysteine concentration). As described in the experimental section,

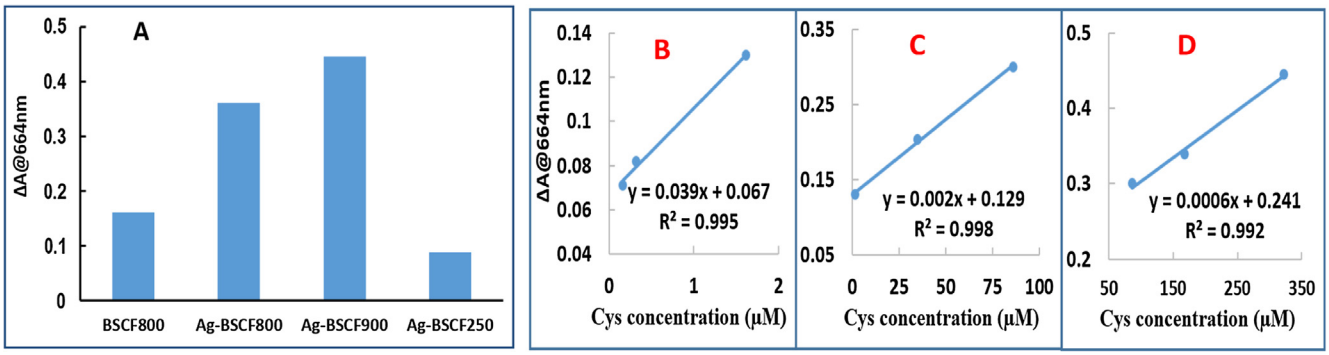

Fig. 2. Absorbance difference of methylene blue at 664 nm (ΔA_{664}) in reaction solutions without L-cysteine and with [L-cysteine] = 80 μM (A). $\Delta A_{664} = A_0 - A_1$, where A_0 and A_1 are the MB absorbance of the reaction solutions in the absence and presence of Cys. Reaction conditions: 50 μL powder solution (1 g/L) + 50 μL L-cysteine (4 mM) + 500 μL MB (10 ppm) + 20 μL PMS (50 mM) incubated at room temperature for 3 min. The final powder concentration was 0.08 g/L, [MB] = 8 ppm, [PMS] = 1.6 mM. The plots of ΔA_{664} versus the Cys concentration using Ag-BSCF900 sample as a catalyst (B–D).

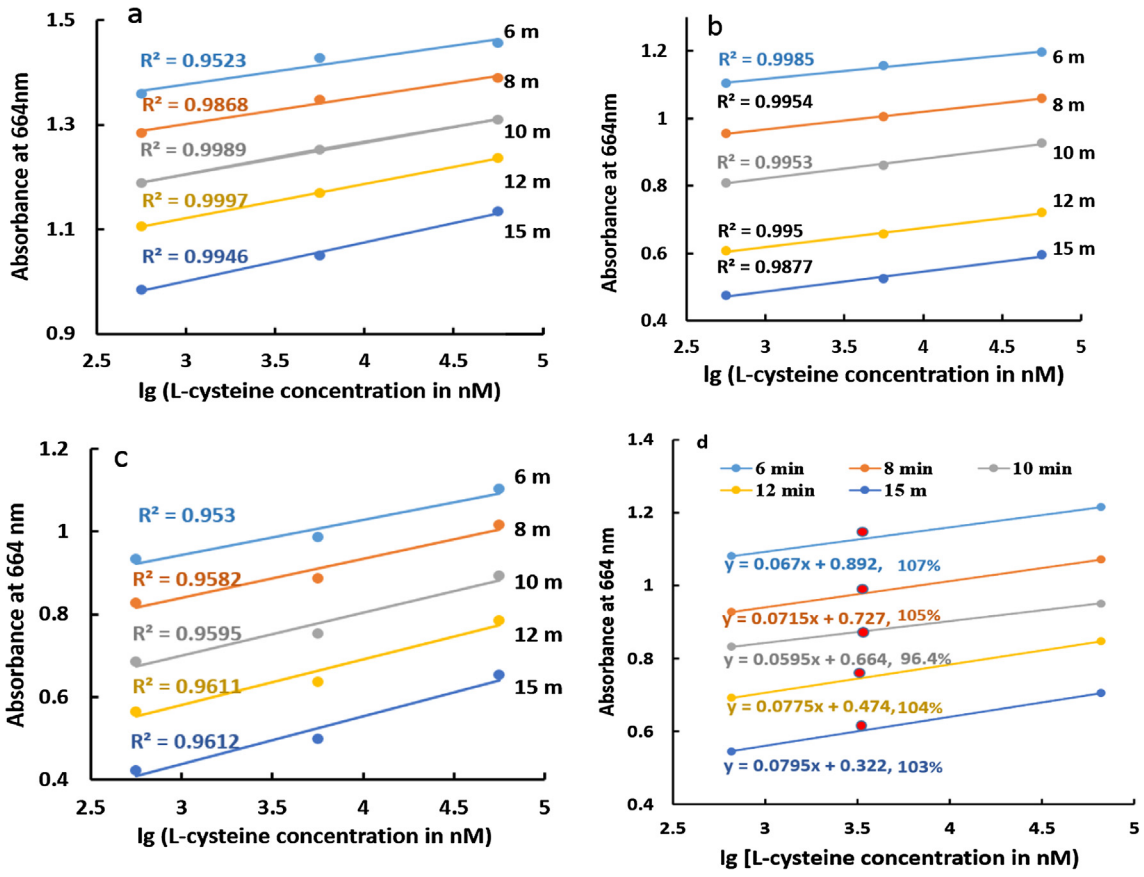

Fig. 3. Influences of Ag-BSCF900 content on the linear response of logarithm of L-cysteine concentration in nM. Experimental investigation was performed in deionised water at room temperature. The concentrations of Ag-BSCF catalyst were 0.025 (a), 0.04 (b), and 0.07 g/L (C), respectively. According to the calibration curves at different reading time, the concentration of spiked 3.2 μM was determined with an acceptable recovery range (96.4–107%) (d).

all the reactants were mixed in the reaction vessel at the beginning of the process (t = 0). After 3 min of incubation and 1 min of centrifugation, 200 μL solution was transferred to a 96-well plate for absorbance reading. At the loading of [Ag-BSCF900] = 0.025 g/L, a liner equation ($R^2 \geq 0.99$) can be maintained from 10 to 12 min (Fig. 3A). When the loading of [Ag-BSCF900] = 0.04 g/L, we can observe a linear response from 6 to 12 min (Fig. 3B). However, there is no linear response when the loading of [Ag-BSCF900] = 0.07 g/L was used (Fig. 3C). The optimum reaction conditions of the Ag-BSCF-Methylene blue-PMS system were thus obtained as follows: 50 μL Ag-BSCF900 solution (0.5 g/L), 50 μL L-cysteine, 500 μL methylene blue (20 ppm) and 10 μL PMS (50 mM). Noteworthy, due to the fast decolourisation rate, two known concentration samples should be included to guarantee the reliability of this method. The feasibility of this sensing system was evaluated by using 3.2 μM spiked Cys. As shown in Fig. 3D, the recovery of all samples was in the range of 96.4–107%, indicating the reliable and accurate detection of Cys.

So far, all the peroxidase-like NPs are reported to decompose H_2O_2 into hydroxyl radicals and then to oxidise colourless substrate TMB or ABTS to generate a blue or green product [30]. Ag-BSCF900 particles may function as peroxidase mimics by

decomposing PMS into both ·OH and $SO_4^{\cdot-}$ and then degrading a dye to colourless products. The catalytic mechanism is confirmed by EPR results as shown in Fig. 4. No obvious signals of the radicals were observed when DMPO alone or DMPO plus PMS solutions were tested.

The fourfold characteristic peaks with an intensity ratio of 1:2:2:1 were consistent with these of DMPO–OH adducts. The typical DMPO–SO_4 adducts were also shown in the EPR spectra of Ag-BSCF900/PMS systems. The signal could be still maintained in a strong intensity after 10 min reaction.

Based on the above results and mechanisms proposed for homogeneous Co^{2+}/PMS and Fe^{3+}/PMS systems, the activation of PMS by Ag-BaSrCoFe perovskite might follow the equations as below (1)–(8) [22,31].

$$Co^{2+} + H_2O \rightarrow CoOH^+ + H^+ \quad (1)$$

$$CoOH^+ + HSO_5^- \rightarrow CoO^+ + SO_4^{\cdot-} + H_2O \quad (2)$$

$$HSO_5^- + \equiv Fe^{3+} \rightarrow \equiv Fe^{2+} + SO_5^{\cdot-} + H^+ \quad (3)$$

$$SO_5^{\cdot-} + SO_5^{\cdot-} \rightarrow 2SO_4^{\cdot-} + O_2 \quad (4)$$

$$HSO_5^- + \equiv Fe^{2+} \rightarrow OH^- + SO_4^{\cdot-} + \equiv Fe^{3+} \quad (5)$$

$$SO_4^{\cdot-} + H_2O \rightarrow H^+ + {\cdot}OH + SO_4^{2-} \quad (6)$$

$$HSO_5^- + Ag^+ \rightarrow Ag^{2+} + SO_4^{\cdot-} + OH^- \quad (7)$$

$$\text{Methylene blue} + SO_4^{\cdot-}/{\cdot}OH \rightarrow \text{decolourised products} \quad (8)$$

The presence of Cys decreased the DMPO-OH and DMPO-SO_4 signal intensities at 5 min. Moreover, both the signals disappeared at 10 min. Instead, a seven-peak DMPOX spectrum was observed due to the DMPO oxidisation [32]. DMPOX intensity was much higher in solution without Cys after 15 min. Therefore, the colour change based on the degradation of dye molecules is the principle for the sensing of the Cys level. Cys molecules attached on Ag nanoparticles and complexed with Co and Fe significantly interfered the radical generation.

To further understand the activation mechanism of PMS by Ag-BSCF900, we used XPS to analyse the sample before and after the decolourisation of MB (Fig. S2). The two main peaks of Co 2p/Ba 3d are shifted to the higher binding energies for the spent catalysts, implying that cobalt valence state increased from Co^{2+} to Co^{3+} due to transferring electrons to PMS to generate $SO_4^{\cdot-}$ [22].

Compared to ·OH, sulfate radicals have been demonstrated to be flexible to a wide pH range with a higher redox potential, and be almost non-selective to all organics [33]. We further extended this strategy by using rhodamine 6G to get a wider linear response range of L-cysteine from 56 nM to 56 μM (Fig. 5). Using the calibration curves from 6 to 15 min, the recoveries of 3.2 μM Cys were calculated to be in the range of 95–100%.

$SO_4^{\cdot-}$ and ·OH can be produced by different combinations of PMS and metal ions (i.e. Cu (I, II) Mn (II, III), Co (II, III), and Fe (II, III)), and various dyes can be degraded to lose colour (i.e. Acid Orange 7, Naphtohol Green B, and Reactive Black B) [34,35]. Based on this, it is possible to find more efficient AOP systems to achieve a better sensitivity. Our future work will focus on uniform perovskite nanoparticle synthesis and fine-tuning the reaction rate for practical detection of Cys.

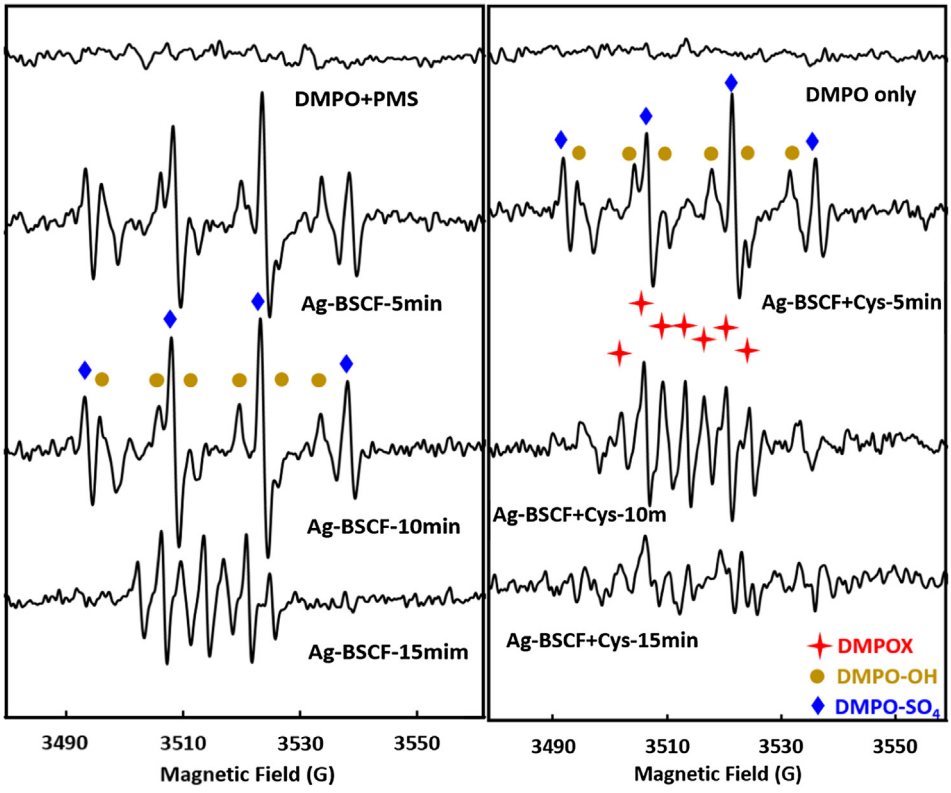

Fig. 4. Comparison of EPR spectra using Ag-BSCF900 with or without L-cysteine. The concentration of Ag-BSCF900 was 0.08 g/L. [L-cysteine] = 40 μM, [PMS] = 0.8 mM. [DMPO] = 25 mM.

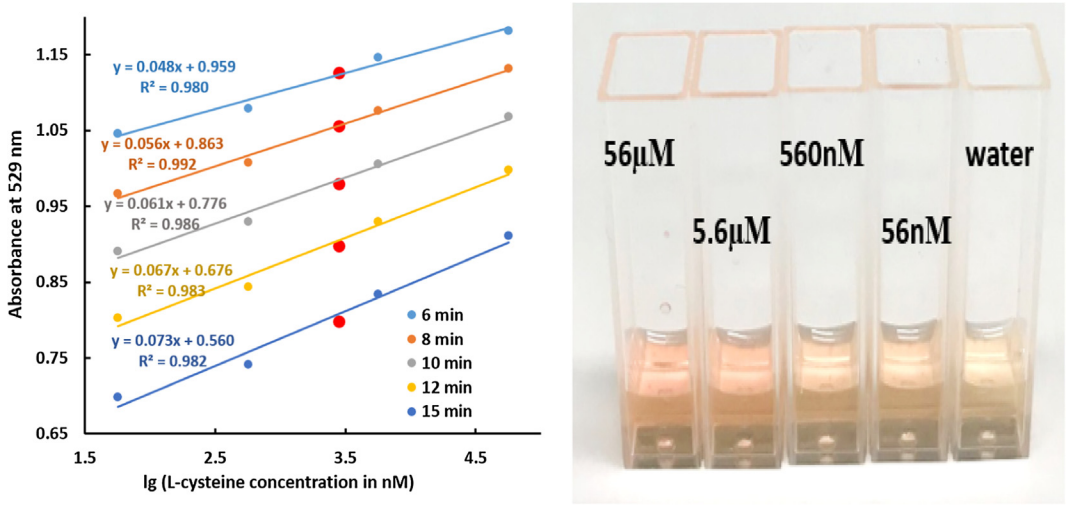

Fig. 5. Calibration curves for L-cysteine detection based on Ag-BSCF900-Rhodamine 6G-PMS system and photographs of the corresponding solutions after 8 min reaction. The concentration of Ag-BSCF900 was 0.035 g/L. [Rho6G] = 17 ppm, [PMS] = 0.7 mM.

4. Conclusions

In summary, we report the first application of a perovskite oxide ($Ba_{0.5}Sr_{0.5}Co_{0.75}Fe_{0.2}O_{3-\delta}$) for sensitive, rapid and facile detection of L-cysteine. The working principle is based on two processes: (1) Ag-BSCF can quickly activate PMS to generate sulfate and hydroxyl radicals for the degradation of dyes and (2) the inhibitory action of Cys conjugated with Ag nanoparticles, Co^{2+} and Fe^{3+} can delay dye decolourisation rate. This finding may extend the advanced oxidation processes (AOPs) of these perovskite oxides from wastewater treatment to bioanalytical sensors.

Appendix A. Supplementary material

Supplementary data to this article can be found online at https://doi.org/10.1016/j.jcis.2019.03.045.

References

[1] R. Li, H. Zhang, J. Ling, C. Huang, J. Wang, Appl. Spectrosc. Rev. 51 (2016) 129.
[2] Y. Yue, F. Huo, P. Ning, Y. Zhang, J. Chao, X. Meng, C. Yin, J. Am. Chem. Soc. 139 (2017) 3181.
[3] G. Chwatko, E. Bald, Talanta 52 (2000) 509.
[4] G. Chen, L. Zhang, J. Wang, Talanta 64 (2004) 1018.
[5] F. Gai, L. Li, Y. Yu, Z. Han, L. Jin, Y. Ao, Y. Liu, Q. Huo, J. Colloid Interface Sci. 529 (2018) 531.
[6] Y. Liu, D. Yu, S. Ding, Q. Xiao, J. Guo, G. Feng, ACS Appl. Mater. Interfaces 6 (2014) 17543.
[7] H. Liu, G. Mei, S. Chen, Y. Long, Anal. Methods 9 (2017) 3249.
[8] L. Xia, Y. Zhao, J. Huang, Y. Gu, P. Wang, Sens. Actuators B Chem. 270 (2018) 312.
[9] Y. He, L. Zheng, ACS Sustain. Chem. Eng. 5 (2017) 9355.
[10] F.A. Silva, M.G. da Silva, P.R. Lima, M.R. Meneghetti, L.T. Kubota, M.O. Goulart, Biosens. Bioelectron. 50 (2013) 202.
[11] H. Huang, X. Liu, T. Hu, P.K. Chu, Biosens. Bioelectron. 25 (2010) 2078.
[12] L. Gao, J. Zhuang, L. Nie, J. Zhang, Y. Zhang, N. Gu, T. Wang, J. Feng, D. Yang, S. Perrett, X. Yan, Nat. Nanotechnol. 2 (2007) 577.
[13] V.K. Singh, P.K. Yadav, S. Chandra, D. Bano, M. Talat, S.H. Hasan, J. Mater. Chem. B 6 (2018) 5256.
[14] Q. Liu, Y. Yang, X. Lv, Y. Ding, Y. Zhang, J. Jing, C. Xu, Sens. Actuators B Chem. 240 (2017) 726.
[15] L. Su, J. Feng, X. Zhou, C. Ren, H. Li, X. Chen, Anal. Chem. 84 (2012) 5753.
[16] X. Lin, H. Deng, G. Wu, H. Peng, A. Liu, X. Lin, X. Xia, W. Chen, Analyst 140 (2015) 5251.
[17] N. Pan, L. Wang, L. Wu, C. Peng, Z. Xie, Microchim. Acta 184 (2017) 65.
[18] H. Bisswanger, Perspect. Sci. 1 (2014) 41.
[19] K. Zhang, C. Zhang, L. Zhao, B. Meng, J. Liu, S. Liu, Energy Fuels 2016 (1829) 30.
[20] Z. Chen, R. Ran, W. Zhou, Z. Shao, S. Liu, Electrochim. Acta 52 (2007) 7343.
[21] C. Jin, X. Cao, F. Lu, Z. Yang, R. Yang, Int. J. Hydrog. Energy 38 (2013) 10389.
[22] X. Duan, C. Su, J. Miao, Y. Zhong, Z. Shao, S. Wang, H. Sun, Appl. Catal. B Environ. 220 (2018) 626.
[23] Y. Chu, X. Tan, Z. Shen, P. Liu, N. Han, J. Kang, X. Duan, S. Wang, L. Liu, S. Liu, J. Hazard. Mater. 356 (2018) 53.
[24] R. Spezia, G. Tournois, T. Cartailler, J. Tortajada, Y. Jeanvoine, J. Phys. Chem. A 110 (2006) 9727.
[25] X. Wu, Y. Xu, Y. Chen, H. Zhao, H. Cui, J. Shen, H. Zhang, RSC Adv. 4 (2014) 64438.
[26] S. Fischer, A.C. Papageorgiou, M. Marschall, J. Reichert, K. Diller, F. Klappenberger, F. Allegretti, A. Nefedov, C. Wöll, J.V. Barth, J. Phys. Chem. C 116 (2012) 20356.
[27] D. Han, X. Tan, Z. Yan, Q. Li, S. Liu, Ceram Int. 39 (2013) 431.
[28] L. Liu, T. Liu, M. Tade, S. Wang, X. Li, S. Liu, Enzyme Microb. Technol. 67 (2014) 53.
[29] J. Jung, D.D. Edwards, J. Solid State Chem. 184 (2011) 2238.
[30] N. Ding, N. Yan, C. Ren, X. Chen, Anal. Chem. 82 (2010) 5897.
[31] F. Song, H. Zhang, S. Wang, L. Liu, X. Tan, S. Liu, Chem. Commun. 54 (2018) 4919.
[32] C. Chen, F. Li, H. Chen, M.G. Kong, Plasmas 24 (2017) 103501, https://doi.org/10.1063/1.4986008.
[33] H. Sun, S. Wang, Catalysis 27 (2015) 209.
[34] D. Chen, X. Ma, J. Zhou, X. Chen, G. Qian, J. Hazard. Mater. 279 (2014) 476.
[35] Y. Huang, Y. Huang, C. Huang, C. Chen, J. Hazard. Mater. 170 (2009) 1110.